Energy Efficient Heat Sink Design: Natural Versus Forced Convection Cooling

Daniel Christen, *Student Member, IEEE*, Milos Stojadinovic, *Student Member, IEEE*, and Juergen Biela, *Senior Member, IEEE*

***Abstract*—In highly efficient converter systems, the power consumption of the cooling system (fans) significantly influences the total system efficiency as well as the power density. This paper investigates the potential of free convection cooled heat sinks and compares their performance to forced convection cooled heat sinks on the basis of their volume and power consumption. Underlying theoretical concepts for both types of cooling systems are summarized and their application in an optimization procedure is presented. The theoretical concepts are validated with prototype heat sinks. Finally, at an example of a half-bridge converter, it is shown that by free convection cooling, not only the efficiency but also the power density can be increased. In this case, by paralleling semiconductor devices the losses decrease approximately by a factor of three while simultaneously the heat sink volume can be reduced by approximately 50%.**

***Index Terms*—Analytical modeling, forced convection, heat sink modelling, natural convection, pareto optimization, thermal management.**

I. Introduction

DUE to the reduced switching losses of modern power semiconductors (e.g., Si/SiC MOSFETs & GaN HEMT), system efficiencies up to 99.5% can be achieved. Nevertheless, in power electronic systems, semiconductor devices are one of the major loss sources and the required cooling system contributes significantly to the total volume. Furthermore, in such highly efficient converters, the cooling system not only has an impact on the overall volume but also influences the total system efficiency in case of forced air cooling. As a consequence, besides the geometrical optimization of the heat sink minimizing the thermal resistance with respect to its volume, the power demand of the cooling system also has to be taken into account.

Various different types of heat sinks have been studied in the past [1]–[3], where the focus of this paper is on air cooled finned (parallel plate) aluminum heat sinks, which are the most commonly used heat sinks in power electronic converters due to their simple and low-cost design. Based on [4], Drofenik *et al.* [5], [6] describe an optimization routine minimizing the thermal resistance of the heat sink with respect to the fan characteristic and the heat sink geometry. In [7], this approach is improved by applying a more accurate heat sink model derived in [8]–[10] and taking additional pressure losses [11] into account. The influence of internal geometry of the heat sink on the pumping power is discussed in [12] and [13]. The importance of the pumping power is reported in [14] and provides an analytical optimization approach considering various duct shapes maximizing the heat transfer density and extend the consideration on the mechanical (pumping) power. However, the electrical efficiency of commercially available fans is not constant for different pumping powers, which is why in this paper the concept proposed in [7] has been complemented with the electrical power required for the cooling system (fans in this paper).

Due to the high system efficiency, natural convection cooling also becomes an attractive option, since in such highly efficient converter systems, the required thermal resistance could be relatively high and accordingly natural convection heat sinks are sufficient. In addition, natural convection cooling could also be beneficial from a volume point of view since no fan is required. Several modeling concepts for natural convection in vertical finned heat sinks are described in [2], [15]–[20]. Due to its compactness, the modeling concepts reported in [2] and [15] are used to investigate the performance boundary between forced and natural convection cooling in this paper. These approaches are extended by additional radiative and convective elements [2], [4] of the heat sink and the electronics to predict the thermal resistance for natural convection cooled heat sinks.

In addition, the trade off between the thermal resistance of the heat sink (heat sink volume & fan losses) and the temperature dependent conduction losses of the semiconductor devices is investigated with the heat sink optimization procedure presented in this paper.

Section II recapitulates the theoretical background for forced convection cooling, which is extended by the fan losses (Section II-A) and free (natural) convection cooling (Section II-B). The resulting limitations of forced convection cooling as well as the potential of free convection cooling are discussed in Section III—first for a fixed junction temperature of the devices and second for a variable junction temperature. The theoretical models are experimentally validated and the measurement results are shown in Section IV.

Manuscript received May 24, 2016; revised August 30, 2016 and October 28, 2016; accepted December 5, 2016. Date of publication December 15, 2016; date of current version June 23, 2017. Recommended for publication by Associate Editor T. M. Lebey.

D. Christen and M. Stojadinovic are with the Departement Informationstechnologie und Elektrotechnik, Eidgenossische Technische Hochschule Zurich, Zurich 8092, Switzerland (e-mail: christen@hpe.ee.ethz.ch; stojadinovic@hpe.ee.ethz.ch).

J. Biela is with the Department of Information Technology and Electrical Engineering, ETH-Zurich, Zurich 8092, Switzerland (e-mail: jbiela@ethz.ch).

Color versions of one or more of the figures in this paper are available online at http://ieeexplore.ieee.org.

Digital Object Identifier 10.1109/TPEL.2016.2640454

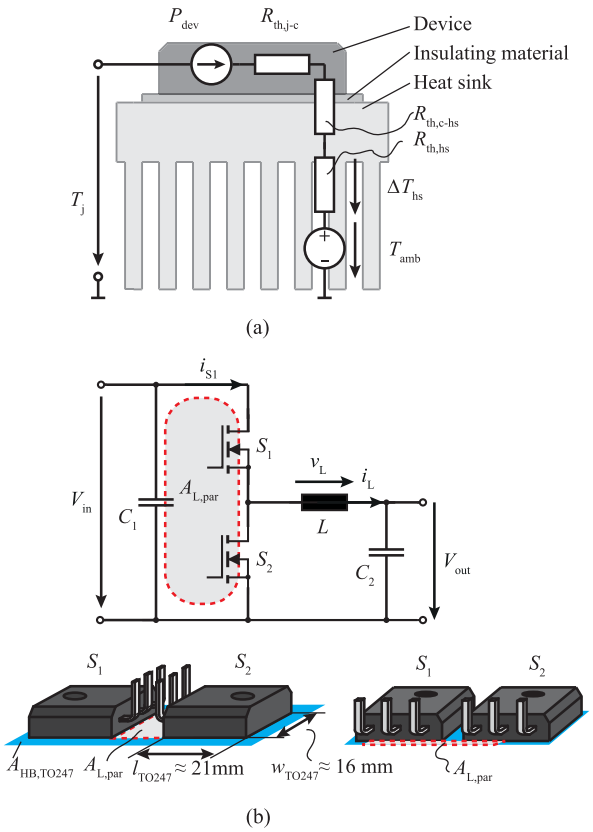

Fig. 1. Considered heat sink design for the optimization (a) represents the underlying thermal circuit equivalent to determine $R_{th,hs}$ and (b) depicts the typical arrangement of the semiconductor devices to minimize the parasitic stray inductance.

II. Heat Sink Modeling

The losses generated in the semiconductor devices (P_{semi}, total conduction, and switching losses) have to be dissipated to the ambience via a heat sink, which usually significantly affects the system volume. The losses in one semiconductor device P_{dev} are dissipated via the series connection of the internal thermal resistance of the device $R_{th,j-c}$ and the thermal resistance of the electrical insulating material between the device and the heat sink $R_{th,c-hs}$ to the heat sink as shown in Fig. 1(a). There, the different loss shares of the devices sum up and are transferred via the heat sink to the ambient, where the transfer resistance of the heat sink $R_{th,hs}$ defines the temperature rise of the heat sink ΔT_{hs}. The maximal allowed thermal resistance of the heat sink $R_{th,hs,\max}$ to keep the junction temperature T_j of the semiconductors below the maximum allowed device temperature $T_{j,\max}$ at the considered ambient temperature T_{amb} is calculated by

$$R_{th,hs,\max} = \frac{T_{j,\max} - \overbrace{P_{\text{dev,max}}\left(R_{th,j-c} + R_{th,c-hs}\right)}^{\Delta T_{j-h,\max}} - T_{\text{amb}}}{P_{\text{semi}}}. \tag{1}$$

There, the maximum losses occurring in a single device $P_{\text{dev,max}}$ define the device specific temperature rise $\Delta T_{j-h,\max}$. In the optimization for air cooled heat sinks in Section III, this $R_{th,hs,\max}$ is the limiting parameter to achieve a thermally feasible design.

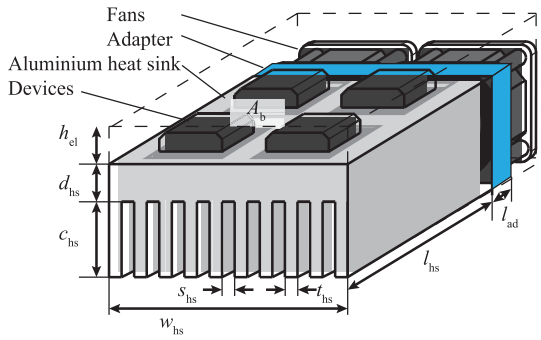

Fig. 2. Heat sink geometry of the forced convection heat sink considered in this paper.

TABLE I
Physical Constants @ 60 °C

Thermal conductivity of air	λ_{air}	0.0285 W/(m K)
Kinematic viscosity of air	ν_{air}	$1.89 \cdot 10^{-5}$ m^2/s
Density of air	ρ_{air}	1.07 kg/m^3
Expansion coefficient	β_{air}	$3.0 \cdot 10^{-3}$ K^{-1}
Thermal capacitance of air	c_{air}	$1.01 \cdot 10^3$ J/(kg K)
Prandtl number for air	Pr	0.71
Thermal conductivity (Al)	λ_{hs}	210 W/(m K)
Emissivity Al, anodize black	$\epsilon_{\text{rad},hs}$	$\approx$0.95 , polished ≈ 0.05
Stefan–Boltzmann constant	σ	$5.6703 \cdot 10^{-8}$ W/(m^{2}K^4)
Gravitational acceleration	g	9.81 m/s^2

For transferring the heat to the ambient here, two types of air cooling are distinguished: forced air cooling and free (natural) convection cooling. For both types of cooling, the thermal resistance of the heat sink $R_{th,hs}$ is determined based on analytical and empirical equations which take the geometrical parameters (heat sink width w_{hs}, length l_{hs}, fin height c_{hs}, channel width s_{hs}, and fin width t_{hs}, Fig. 2) into account. In the following, the underlying analytical models presented in [2], [7], [10], and [15] are briefly summarized for completeness and extended by the power consumption of the cooling system.

For both types of cooling, the lower limit of the baseplate area A_b (see Fig. 2) is defined by the number of semiconductor devices which have to be mounted on the heat sink. Furthermore, to achieve a small stray inductance in the commutation path of the half-bridge, the area between the devices of the bridge leg $A_{L,\text{par}}$ has to be minimized [see Fig. 1(b)]. This results in a typical minimal basic cell area, which is exemplarily for the TO-247 package $A_{\text{HB,TO247}} \approx 20$ mm $\times$ 60 mm. In dependence of the number of paralleled half-bridge cells n_{semi}. multiples of these basic cells have to be placed on the heat sink. The baseplate area is extended to a maximum of twice the semiconductor area. Thus, heat spreading effects in the baseplate are neglected

$$n_{\text{semi}} \cdot A_{\text{HB,TO247}} < A_b < 2 \cdot n_{\text{semi}} \cdot A_{\text{HB,TO247}}. \tag{2}$$

In the following sections the heat sink modelling is discussed. The underlying physical constants used in the following considerations of air cooled systems are listed in Table I.

A. Forced Convection Cooling

There are many thermal heat sink modeling and optimization procedures for forced convection heat sinks discussed in the past, whereas this paper will stay close to the discussion presented in [5]–[7], [10] for finned heat sinks (see Fig. 2). First, the thermal modeling of the heat sink's thermal resistance will be summarized, followed by the pressure drop shares of the different heat sink parts. Finally, the link to the power consumption of the fan is presented.

1) Thermal Modeling: To determine the thermal resistance of a certain heat sink geometry in dependance of the volumetric flow, the three-dimensional (3-D) problem is reduced to a 2-D problem based on a thermal network analysis and under the assumption of equally distributed power losses on the baseplate. There, two thermal resistances are distinguished, the thermal resistance of the heat sink baseplate $R_{th,d}$, and the thermal resistance of the finned part $R_{th,\text{fin}}$. The thermal resistance $R_{th,d}$ is approximated by only taking the heat conduction in the baseplate into account

$$R_{th,d} = \frac{d_{hs}}{w_{hs} l_{hs} \lambda_{hs}}. \tag{3}$$

Heat spreading effects in the baseplate are neglected.

To quantify the thermal transfer resistance from the heat sink to the ambient, first the average thermal transfer coefficient α_{fc} has to be determined which defines the thermal resistance per surface area. Based on the work presented in [8]–[10], Gammeter *et al.* [7] improved the work presented in [5] and derived a new procedure to determine $R_{th,hs}$. There, the Nusselt number $Nu_{\sqrt{A}}$, which characterizes the thermal transition from solid to fluid matter, of a channel with an arbitrary cross section area is determined based on the square root of a single air channel

$$Nu_{\sqrt{A}} = \left[\left(\frac{C_4 F_{Pr}}{\sqrt{z^*}} \right)^m + \left(\left(C_2 C_3 \left(\frac{F_{Re_{\sqrt{A}}}}{z^*} \right)^{1/3} \right)^5 + \left(C_1 \frac{F_{Re_{\sqrt{A}}}}{8\sqrt{\pi}\epsilon^\gamma} \right)^5 \right)^{m/5} \right]^{1/m} \tag{4}$$

Under the assumption of uniform wall temperatures, the coefficients, used to calculate $Nu_{\sqrt{A}}$, found in [7] and [8] are

$$C_1 = 3.24 \qquad C_2 = 3/2 \qquad C_3 = 0.409 \qquad C_4 = 2$$

$$\gamma = \frac{-3}{10} \qquad m = 2.27 + 1.65 Pr^{1/3}$$

and the characteristic geometrical parameters ϵ (channel aspect ratio) and z^* (dimensionless axial position) are

$$\epsilon = \frac{s_{hs}}{c_{hs}} \qquad z^* = \left. \frac{z \nu_{\text{air}}}{\dot{m} \cdot v_{\text{avg}} \cdot A \cdot Pr} \right|_{(z \to l_{hs})} = \frac{l_{hs} n_{\text{fin}} \nu_{\text{air}}}{Pr \cdot \dot{V}}$$

The Prandtl number Pr, linking the viscosity and thermal conductivity of a fluid, and the Reynolds number, characterizing the kind of flow (laminar/turbulent), are taken by the Prandtl number function F_{Pr} and the friction factor Reynolds number product $F_{Re_{\sqrt{A}}} = f_{fr} \cdot Re_{\sqrt{A}}$ into account in (4)

$$F_{Pr} = \frac{0.564}{\left(1 + \left(1.664 Pr^{1/6}\right)^{9/2}\right)^{2/9}} \tag{5}$$

$$F_{Re_{\sqrt{A}}} = \sqrt{\frac{11.8336 \dot{V}}{l_{hs} n_{\text{fin}} \nu_{\text{air}}} + \left(\frac{12}{\sqrt{\epsilon}(1+\epsilon)(1 - \frac{192}{\pi^5}\epsilon \tanh\left(\frac{\pi}{2\epsilon}\right))} \right)^2}. \tag{6}$$

Depending on $Nu_{\sqrt{A}}$, the heat transfer coefficient α_{fc} of a defined heat sink for different volume flows $\dot{V}$ can be determined by

$$\alpha_{fc} = \frac{Nu_{\sqrt{A}} \lambda_{\text{air}}}{d_h}. \tag{7}$$

With the effective surface area A_{eff}[1](described in [7] and [21]) of the channels contributing to the heat transfer

$$A_{\text{eff}} = (n_{\text{fin}} - 1)(2 c_{hs} \eta + s_{hs}) l_{hs} \tag{8}$$

$$\eta = \frac{\tanh(f)}{f} \quad \text{with} \quad f = \sqrt{\frac{\alpha_{fc} 2 (t_{hs} + l_{hs})}{\lambda_{hs} t_{hs} l_{hs}}} c_{hs} \tag{9}$$

the thermal resistance of the fins $R_{th,\text{fin}}$ as function of the volume flow $\dot{V}$ is given by

$$R_{th,\text{fin}}(\dot{V}) = \frac{1}{\rho_{\text{air}} c_{\text{air}} \dot{V} \left(1 - e^{-\frac{\alpha_{fc} A_{\text{eff}}}{\rho_{\text{air}} c_{\text{air}} \dot{V}}}\right)}. \tag{10}$$

The thermal resistance of the heat sink $R_{th,hs}$ is the series connection of thermal resistances of the baseplate and the fins

$$R_{th,hs} = R_{th,d} + R_{th,\text{fin}}. \tag{11}$$

2) Pressure Drop Considerations: As mentioned before, the thermal resistance $R_{th,hs}$ strongly depends on the volumetric flow $\dot{V}$ through the channels and thus on the operating point of the fan. The operating point of the fan is determined by intersecting the characteristics of the heat sink and of the fan [see Fig. 3(a)]. To determine the $\Delta p - \dot{V}$ characteristic of the heat sink, several effects causing a pressure drop Δp have to be considered [7], [11] including the pressure drop due to the fluid acceleration, the friction of the channel, and sudden contraction/expansion at the heat sink inlet and outlet. The pressure drop in the heat sink channels with hydraulic diameter $d_h = (2 s_{hs} c_{hs})/(s_{hs} + c_{hs})$ is determined according to [11] by

$$\Delta p_{hs} = \left(f_{fr} \frac{l_{hs}}{d_h} + K_{se} + K_{sc} \right) \frac{\rho_{\text{air}}}{2} \frac{\dot{V}^2}{((n_{\text{fin}} - 1) s_{hs} c_{hs})^2}. \tag{12}$$

For the cross section adapter, the pressure drop is

$$\Delta p_{ad} = \left(f_{fr,ad} \frac{l_{ad}}{d_{h,ad}} \frac{1}{4} + K_{\text{vent}} \right) \frac{\rho_{\text{air}}}{2} \frac{\dot{V}^2}{(w_{hs} c_{hs})^2} \tag{13}$$

and due to the acceleration of the fluid

$$\Delta p_{\text{acc}} = \left(\frac{1}{((n_{\text{fin}} - 1) s_{hs} c_{hs})^2} - \frac{1}{(h_{\text{fan}} w_{hs})^2} \right) \frac{\rho_{\text{air}} \dot{V}^2}{2}. \tag{14}$$

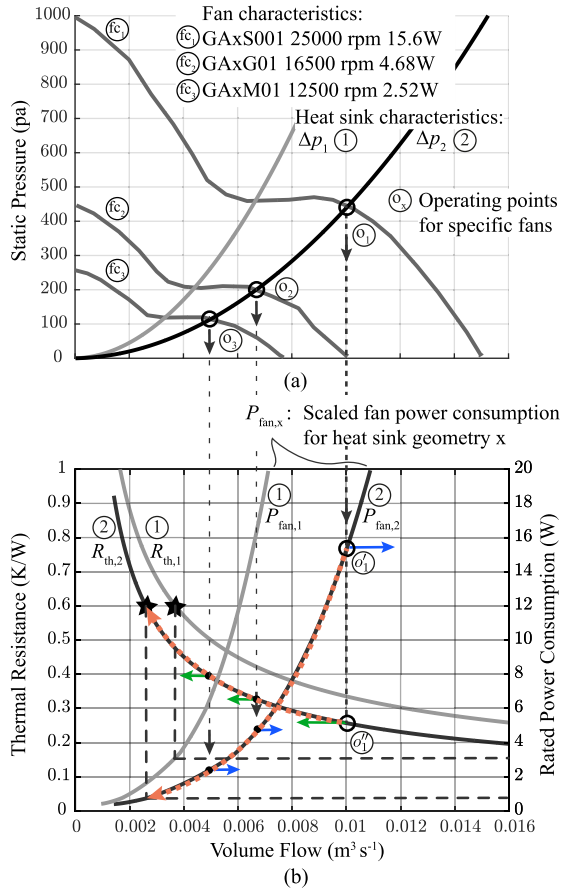

Fig. 3. Procedure to determine the dependency of R_{th} on P_{fan} based on the fan laws: (a) Typical fan characteristics ($fc_1 - fc_3$) intersected with the $\Delta p - \dot{V}$ characteristic of the two prototype heat sinks (see ①&② Section IV) to determine the operating point (e.g., $o_1 - o_3$) of the cooling system. (b) Achievable $R_{th,hs}$ (e.g. o_1'') and the respective P_{fan} (e.g. o_1') are depicted for a reference fan (e.g., fc_1). By applying the fan laws (16)–(18) and (19), the required P_{fan} to achieve $R_{th} = 0.6$ K/W for these heat sinks can be directly determined (red dashed).

The detailed explanations and expressions for the loss and friction factors (K_{se}, K_{sc}, K_{vent}, f_{fr} and $f_{fr,ad}$) can be found in [7] and [10].

By summing up the different pressure drops, the overall pressure drop Δp_{sum} in dependence of $\dot{V}$ of the considered heat sink results

$$\Delta p_{\text{sum}} = \Delta p_{hs} + \Delta p_{ad} + \Delta p_{\text{acc}} \approx K_{\text{tot}} \cdot \dot{V}^2. \tag{15}$$

There, the pressure drop of the cooling system increases approximately quadratically with increasing volumetric flow. The general loss factor K_{tot} combines the different loss factors discussed above. Fig. 3(a) illustrates the two heat sink $\Delta p - \dot{V}$ characteristics for the prototype systems shown in Section IV.

3) Fan Analysis: There are several dependencies of the fan $\Delta p - \dot{V}$ characteristic, like rotor blade angle, fan geometry, and speed, which have to be taken into account. Since the required detailed geometrical data are not always available, this paper focuses on fans of the size 40 mm $\times$ 40 mm $\times$ 28 mm from different manufacturers (Delta Electronics, NMB, Sanyo Denki), which are compact and provide a high diversity concerning

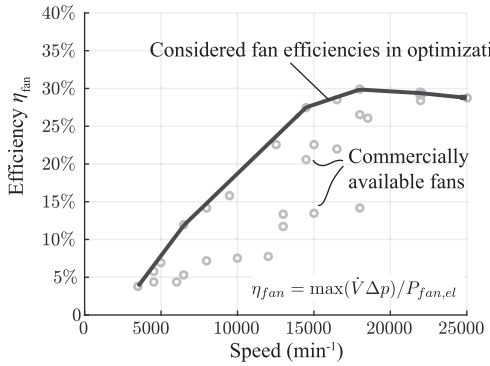

Fig. 4. Efficiency of typical 40 mm $\times$ 40 mm $\times$ 28 mm fans as function of the speed. The efficiency of the commercially available fans (e.g., NMB, Sanyo Denki, EBM) are marked by circles.

speed, static pressure head, and volumetric flow. Furthermore, these fans already have a integrated flow guidance of roughly 1 cm, thus the minimum adapter length to avoid static pressure drop degradation of 3 cm, assumed in [7], is reduced to 2 cm. Three typical fan characteristics (fc_1, fc_2, fc_3) are shown in Fig. 3(a). The characteristic of geometrical similar fans scale with the fan laws and/or affinity laws [22]–[25] what was checked based on datasheet values, where m is the fan speed

$$\dot{V}_2 = \dot{V}_1 \cdot \frac{m_2}{m_1} \tag{16}$$

$$\Delta p_2 = \Delta p_1 \cdot \left(\frac{m_2}{m_1}\right)^2 \tag{17}$$

$$P_{m,2} = P_{m,1} \cdot \left(\frac{m_2}{m_1}\right)^3 = \dot{V}_2 \cdot \Delta p_2. \tag{18}$$

According to these laws, a quadratic dependency of the static pressure head on the volume flow can be observed. Since the $\Delta p - \dot{V}$ characteristic of a specific heat sink also shows this quadratic behavior (see (15)), the operating point of the cooling system is always on the same relative position on the fan characteristic in dependence of the speed [see intersecting points of the characteristics $o_1 - o_3$ in Fig. 3(a)].

The mechanical power $P_m = \Delta p \cdot \dot{V}$ varies to the power of three referring to the fan speed and strongly depends on the operating point. However, for a certain fan speed, the electrical power consumption is relatively constant [26], [27]. Thus, the maximum mechanical power $P_{m,\max}$ is linked by an efficiency coefficient η_{fan} to the electrical power consumption of the fan

$$P_{\text{fan},el} = \eta_{\text{fan}} \cdot P_{m,\max} \tag{19}$$

To determine η_{fan}, datasheets of several fans have been analyzed (see Fig. 4). The fan efficiency varies relatively strong and drops with decreasing fan speed. In the following optimization procedure, the highest achievable fan efficiency has been considered.

Referring to the laws (16)–(18) and assuming an approximately constant power consumption of the fan at a certain fan speed [e.g., fc_1 in Fig. 3(a)], allows to recalculate the $R_{th,hs}$ in dependence of the power consumption of the fan for a specific

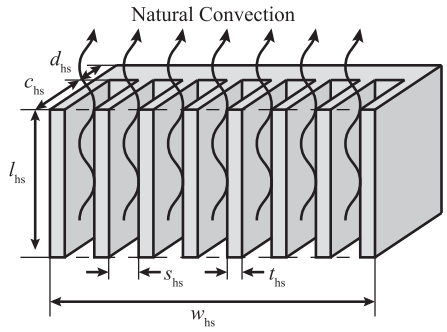

Fig. 5. Geometrical parameters of the considered vertical finned free convection heat sink.

heat sink geometry. For example, in Fig. 3, from the reference operating point o_1, the power consumption o_1' and the R_{th} o_1'' can be determined. By applying the fan laws, the dependency of $R_{th,hs}$ on the pumping power $P_{\rm fan}$ can be derived. This allows to scale $P_{\rm fan}$ such that the desired R_{th} is achieved for a given heat sink geometry [red dashed in Fig. 3(b)].

Furthermore, it can be seen that high fan power levels (10—20 W) do not significantly decrease the thermal resistance anymore while at low fan powers, the sensitivity of the $R_{th,hs}$ on $P_{\rm fan}$ is relatively high.

B. Free Convection Cooling

Without fan, the heat is transferred by free convection and radiation to the ambient. This paper focus on vertical parallel finned heat sinks as illustrated in Fig. 5, whereas first the theory to calculate the convective heat transfer by the fins is summarized followed by the impact of other convective parts of the heat sink and the heat transfer by radiation.

1) Convective Heat Transfer by the Fins: In [2], [15]–[17], and [20], analytical models for vertical parallel finned heat sinks, as illustrated in Fig. 5, are derived. This paper focus on the modeling approach proposed in [15] due to its compactness. There, an uniform fin temperature is assumed due to the relatively low thermal resistance inside the heat sink. The heat-transfer coefficient for natural convection α_{nc} is related to the Nusselt number Nu_Γ by

$$Nu_\Gamma = \frac{\alpha_{nc}\Gamma}{\lambda_{\rm air}} \tag{20}$$

with the characteristic length [15]

$$\Gamma = \frac{2c_{hs}s_{hs}}{2c_{hs}+s_{hs}} \tag{21}$$

which characterizes a certain geometry. To determine Nu_Γ for natural convection in a first step, the modified Rayleigh number Ra_Γ [15] respective to the characteristic length has to be determined which characterizes the heat transfer within a fluid in dependence of the temperature difference and the length

$$Ra_\Gamma = \frac{\Gamma}{l_{hs}} Gr_\Gamma Pr. \tag{22}$$

The Rayleigh number is depending on the Prandtl number Pr and the Grashof number Gr_Γ. The Pandtl number defines the ratio between thermal conductivity and viscosity of a fluid and is approximately constant $Pr = 0.71$ for air in the considered temperature range. The modified Grashof number Gr_Γ characterizes the dynamic (buoyancy versus viscous force) of the fluid (here air) and is determined by

$$Gr_\Gamma = \frac{g\beta_{\rm air}\Delta T \Gamma^3}{\nu_{\rm air}^2}. \tag{23}$$

Based on these characteristic numbers Ra_Γ and Gr_Γ, Nu_Γ is given by

$$Nu_\Gamma = \frac{Ra_\Gamma}{\Psi}\left(1-\exp\left(-\Psi\left(\frac{0.5}{Ra_\Gamma}\right)^{3/4}\right)\right) \tag{24}$$

$$\Psi = \frac{24(1-0.483e^{-17/\epsilon})}{\left(1+\frac{\epsilon}{2}\right)\left(1+(1-e^{-0.83\epsilon})(9.14\epsilon^{1/2}e^{-464s_{hs}}-0.61)\right)^3} \tag{25}$$

where $\epsilon = s/c$ is the channel aspect ratio. The surface area of the finned heat sink is

$$A_{\rm sur,fin} = (n_{\rm fin}-1)(s_{hs}+2c_{hs})l_{hs}. \tag{26}$$

The resulting thermal resistance of the finned part of the heat sink for the natural convection is

$$R_{th,\rm fin} = \frac{1}{\alpha_{nc}A_{\rm sur,fin}} = \frac{\Gamma}{Nu_\Gamma \lambda_{\rm air} A_{\rm sur,fin}}. \tag{27}$$

2) Additional Convection: Other parts of the heat sink or devices are also exposed to the ambient and thus have to be considered in the calculation. Most of these surfaces are arranged in a horizontal or vertical way and can be approximated by flat plates. The corresponding equations to estimate the thermal convection of vertically arranged plates (characteristic length $\Gamma = l_{pl}$) with a constant surface temperature [2] are

$$Nu_{pl} = \left((Nu_l)^m + (Nu_t)^m\right)^{1/m}. \tag{28}$$

There, the two flow regimes, laminar (Nu_l) and turbulent (Nu_t), are distinguished

$$Nu_l = \frac{2}{\ln(1+2/Nu_T)} = \frac{2}{\ln(1+2/(C_l\cdot Ra^{1/4}))} \tag{29}$$

$$Nu_t = \frac{C_t Ra^{1/3}}{1+1.4\cdot 10^9\cdot Pr/Ra} \tag{30}$$

$$Ra = \frac{g\,\beta_{\rm air}\,Pr\,\Delta T\,l_{pl}^3}{\nu_{\rm air}^2} \tag{31}$$

$$m = 6 \qquad C_l = 0.103 \qquad C_t = 0.515.$$

The thermal resistance of a vertical plate with length l_{pl} (vertical dimension) is given by

$$R_{th,pl} = \frac{l_{pl}}{A_{pl}Nu_{pl}\lambda_{\rm air}} = \frac{1}{w_{pl}Nu_{pl}\lambda_{\rm air}}. \tag{32}$$

Similar equations for a horizontal plate arrangement can be found in [2]. Since in most cases, the arrangement and the kind of the electronics is unknown, for the optimization it is assumed that only the finned part of the heat sink is contributing in the heat transfer to the ambient. However, as the measurements in

Section IV show, additional convection has a strong impact on the thermal resistance and thus have to be considered in the final evaluation of heat sinks for known applications.

3) Radiation: Commercially available heat sinks are often black anodized to improve the heat transfer by radiation due to the increased emissivity ϵ_{rad}. The outer surface of the finned part of the heat sink is approximated by

$$A_{\mathrm{rad}} = 2 \cdot (l_{hs}(c_{hs} + d_{hs}) + w_{hs}d_{hs}) + l_{hs}w_{hs}. \tag{33}$$

In arbitrary setups additional radiating surfaces have to be considered (e.g., semiconductor devices). Corresponding to the Boltzmann law, the thermal resistance due to the radiation $R_{th,\mathrm{rad}}$ is

$$R_{th,\mathrm{rad}} = \frac{\Delta T}{\dot{Q}} = \frac{T_{hs} - T_{\mathrm{amb}}}{\epsilon_{\mathrm{rad},hs}\sigma A_{\mathrm{rad}}\,(T_{hs}^4 - T_{\mathrm{amb}}^4)} \tag{34}$$

where the temperatures are in Kelvin.

4) Total Thermal Resistance: The parallel connection of $R_{th,\mathrm{fin}}$, $R_{th,pl}$, and $R_{th,\mathrm{rad}}$ results in the total thermal resistance of the heat sink

$$R_{th,nc} = \left(\frac{1}{R_{th,\mathrm{fin}}} + \frac{1}{R_{th,pl}} + \frac{1}{R_{th,\mathrm{rad}}}\right)^{-1}. \tag{35}$$

A general dependency of the thermal resistance on the heat sink volume can be observed, which is in good accordance with the R_{th} achievable by commercially available free convection heat sinks [see Fig. 6(a)]

$$R_{th,nc} = 0.4633 \cdot 10^{-3} \cdot V^{-0.9306} + 0.122. \tag{36}$$

However, the thermal resistance is strongly dependent on the ambient temperature as well as on the temperature difference [see Fig. 6(b)], since with increasing temperature on one hand, the air acceleration and thus the thermal transfer coefficient are improving and on the other hand, the radiation is increasing to the power of four.

III. Optimization Procedure and Results

Based on the previously discussed models, the heat sink can be optimized to achieve a thermal feasible $R_{th,hs}$ as a function of the power consumption of the fan power P_{fan} and the volume of the heat sink V_{hs}. As a common topology in power electronics, the following optimization procedures are discussed for a half-bridge converter (see Fig. 1). The total losses of the half-bridge include P_{semi} and the additional power consumption of the fan P_{fan}. The overall volume of the heat sink V_{hs} includes the volume of the heat sink body and for forced convection cooling, the additional volume of the fan and the cross section adapter at the inlet of the heat sink.

In real applications, additional to the physical volume of the heat sink, also the area for the air intake and the exhaust have to be taken into account. However, how much volume is required for the intake and exhaust of the heat sink is strongly depending on the application, the housing, and the heat sink arrangement. In this paper, it is assumed that the pressure loss before and after the heat sink is small compared to the pressure drop in the cooling system, and therefore, is neglected in this paper.

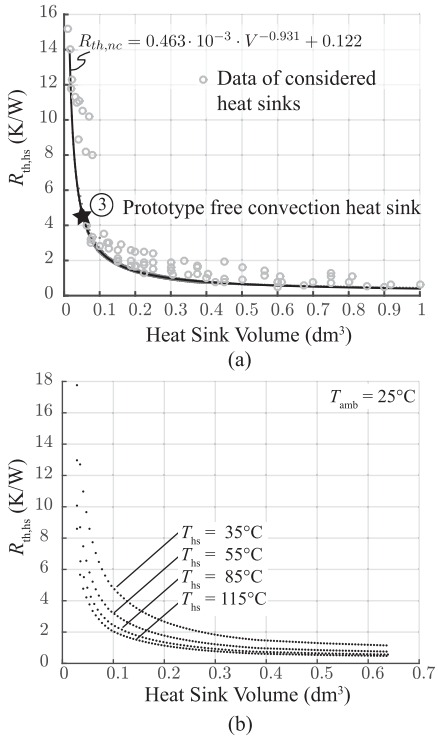

Fig. 6. Dependencies of natural convection cooled heat sinks on the volume and the temperature: (a) Achievable $R_{th,hs}$ of black anodized aluminium heat sinks in dependence of the heat sink volume. The gray dots indicate commercially available heat sinks with similar geometries (e.g., Fischer Elektronik). The ambient and the heat sink temperatures are $T_{\mathrm{amb}} = 25\,°\mathrm{C}$ and $T_{hs} = 85\,°\mathrm{C}$. (b) Achievable $R_{th,hs}$ for natural convection heat sink is strongly temperature dependent. The $R_{th,hs}$ decreases with increasing temperature difference $\Delta T = T_{hs} - T_{\mathrm{amb}}$.

In the following, two possible optimization routines for air cooled heat sinks are discussed. First, the case when the junction temperature T_j of the semiconductor devices is fixed to a constant value is analyzed, since it offers a simple and fast analysis of the losses (see Fig. 7). In a second case, the impact of a higher fan power and the resulting reduced $R_{th,hs}$ and lower T_j on the overall system efficiency is investigated (see Fig. 8).

In both cases, the assumed power electronic system is a half-bridge buck-boost converter (see Fig. 1) whereas the operating parameters can be found in Table II. The applied semiconductor devices are SiC MOSFETs (CMF20120D). There are two loss shares of the semiconductor devices which are considered in this paper. The switching losses P_{sw}, which are assumed to be temperature independent, and the conduction losses P_{cond} for which the temperature dependence of the on-state resistance is taken into account. For the switching losses per device, the turn-on $E_{s,\mathrm{on}}$ and the turn-off $E_{s,\mathrm{off}}$ energy of the devices in dependence of the drain-current are

$$\begin{aligned} E_{s,\mathrm{on}} &= (-0.0042I_{ds}^3 + 4.72I_{ds}^2 + 18.45I_{ds} + 365) \cdot 10^{-7} \\ E_{s,\mathrm{off}} &= (1.83I_{ds}^2 + 1.77I_{ds} + 132) \cdot 10^{-7} \\ P_{sw} &= f_s \cdot (E_{s,\mathrm{on}} + E_{s,\mathrm{off}}) \end{aligned} \tag{37}$$

for the SiC devices in the considered current range. I_{ds} is the current at the switching instant and the data results from loss

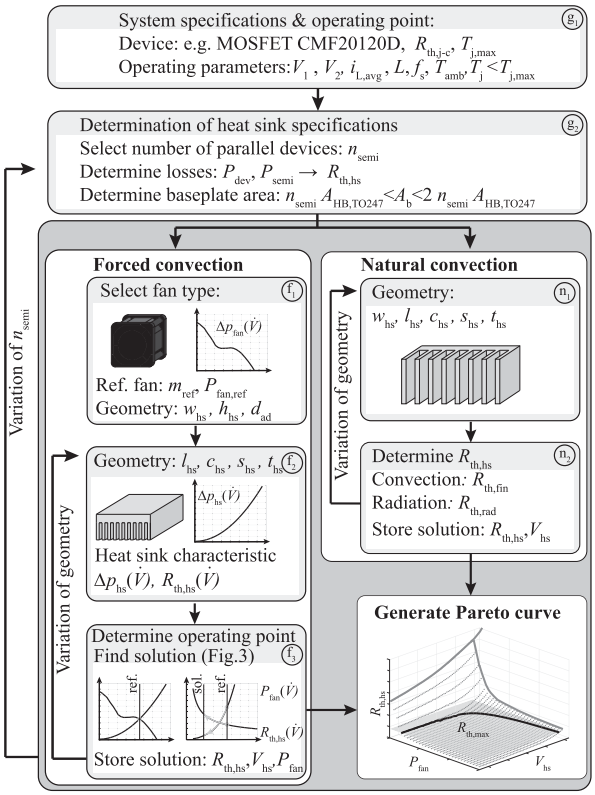

Fig. 7. Optimization procedure for forced and natural convection heat sinks. In the first step g_1, the operating point and the devices are defined. Afterwards in g_2, the required $R_{th,hs}$ is determined in dependence of the number of paralleled semiconductor devices n_{semi} for a predefined junction temperature T_j. For forced convection cooling (f_1–f_3), the tradeoff between volume V_{hs} and the required fan power P_{fan} to achieve $R_{th,hs}$ is determined. Based on a reference fan (here: 40 mm × 40 mm × 28 mm), a reference operating point can be determined for a given heat sink geometry. Finally, in f_3, P_{fan} is scaled to achieve the desired $R_{th,hs}$. Steps f_1–f_3 are repeated for several heat sink geometries what results in different ($R_{th,hs}$, P_{fan}, V_{hs}) solution points. For natural convection cooling, with steps n_1–n_2, the heat sink geometry is varied what results in one optimal solution for a predefined $R_{th,hs}$. Finally, for the required $R_{th,hs}$ a minimal volume V_{hs} in dependence of P_{fan} can be determined what results in a Pareto curve.

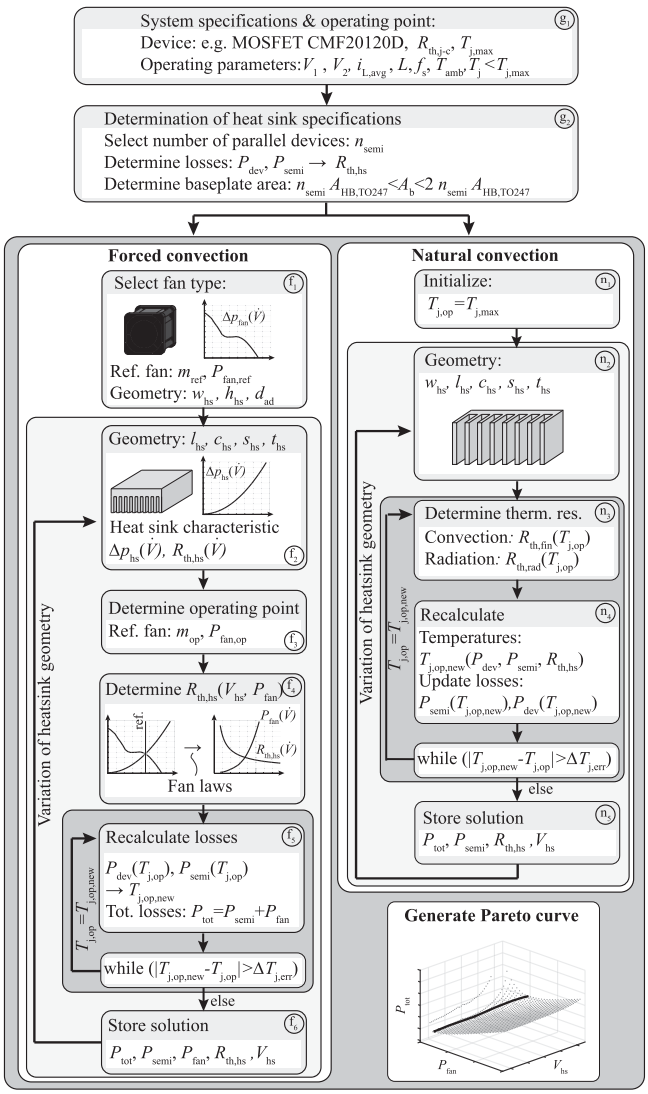

Fig. 8. Adapted heat sink optimization routine presented in Fig. 7 with an internal iteration loop (dark inner boxes). The losses and temperatures have to be iterated until the temperature deviation is below a certain limit. The resulting Pareto surface includes the total power losses in dependence of the of V_{hs} and P_{fan}.

measurements at 400 V [28]. The conduction losses per device are calculated by

$$P_{\mathrm{cond}} = i_{\mathrm{dev,rms}}^2 \cdot R_{ds,\mathrm{on}}(T_j) \tag{38}$$

and the temperature dependency of the on-state resistance $R_{ds,\mathrm{on}}$ can be approximated by

$$R_{ds,\mathrm{on}}(T_j) = R_{\mathrm{ref}}\left(0.96 + 0.81 \cdot 10^{-3} T_j + 2.28 \cdot 10^{-5} T_j^2\right) \tag{39}$$

with $R_{\mathrm{ref}} = 80\ \mathrm{m\Omega}$ @ 25 °C. To determine the total losses of the semiconductor devices in the power converter, the different loss shares have to be summed up

$$P_{\mathrm{semi}} = n_{\mathrm{semi}} \cdot (P_{\mathrm{cond},s1} + P_{sw,s1} + P_{\mathrm{cond},s2} + P_{sw,s2}). \tag{40}$$

The worst case losses generated in a single device are

$$P_{\mathrm{dev,max}} = \max[(P_{\mathrm{cond},s1} + P_{sw,s1}), (P_{\mathrm{cond},s2} + P_{sw,s2})]. \tag{41}$$

TABLE II
OPERATING PARAMETERS OF THE EXAMPLE SYSTEM

Input voltage	V_{in}	400 V
Output voltage	V_{out}	320 V
Duty cycle	D	0.8
Average inductor current	I_L	20 A
Current ripple	Δi_L	10 A
Switching frequency	f_s	50 kHz

Based on the calculated losses and (1), the maximum allowed thermal resistance $R_{th,\mathrm{max}}$ can be determined. The geometric design space for the optimization routines is chosen according to commercially available heat sinks (see Table III [29]).

A. Constant Junction Temperature $T_j = const$

Often in optimization routines for power electronic systems, the junction temperature of the semiconductor devices is

TABLE III
GEOMETRICAL CONSTRAINTS OF HEAT SINK OPTIMIZATION FOR THE EXAMPLE SYSTEM

Heat sink width	w_{hs}	[50 mm . . . 200 mm]
Heat sink length	l_{hs}	[30 mm . . . 200 mm]
Baseplate thickness	d_{hs}	3 mm
Fin height	c_{hs}	[10 mm . . . 50 mm]
Channel width	s_{hs}	[2 mm . . . 10 mm]
Fin width	t_{hs}	[1 mm . . . 5 mm]
Adapter length	l_{ad}	10 mm
Fan dimensions	$w_f \times l_f \times d_f$	40 mm × 40 mm × 28 mm

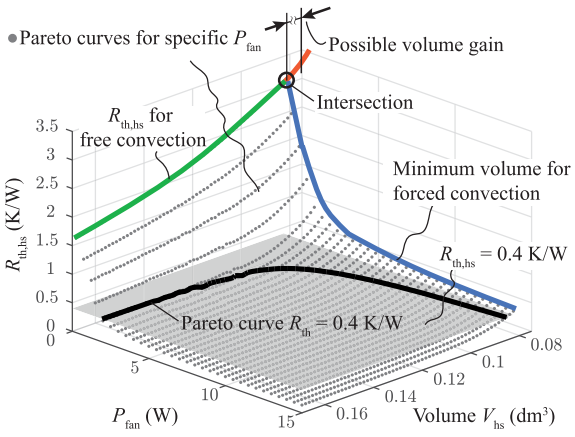

Fig. 9. Shows the boundaries for the minimal $R_{th,hs}$ that can be achieved in dependence of the applied fan power P_{fan} and the mechanical constraints (see Table III). Furthermore, for $R_{th,hs} = 0.4$ K/W, the dependency between volume and P_{fan} is illustrated (black). The circle marks the intersection between mechanical and free convection limit. If a R_{th} higher than this value is required, free convection enables a reduced volume (indicated red).

assumed to be a fixed value below the maximum allowed junction temperature. This constant temperature level T_j is chosen relatively high ($\approx 20\%$ below $T_{j,\max}$) to allow a high $R_{th,\max}$ and thus enabling a small heat sink volume. The respective heat sink optimization routine is depicted in Fig. 7.

Based on the system specifications and the operating point, the losses (P_{semi} & $P_{\mathrm{dev,max}}$) and the respective $R_{th,hs}$ are determined.

To calculate the Pareto front with V_{hs} and P_{fan} as key parameters to achieve the desired $R_{th,hs}$, first a type of fan has to be selected (here: 40 mm × 40 mm × 28 mm). This selection defines the width and maximum height of the heat sink.

Based on this reference fan, a reference operating point and thus a reference thermal resistance $R_{th,hs,\mathrm{ref}}$ for every heat sink geometry within the design space can be determined. To achieve the desired $R_{th,hs}$, the fan power and accordingly the thermal resistance can be directly scaled by the fan laws (see Section II-A).

To evaluate the limit for free convection, in the first step the heat sink temperature has to be determined. In dependence of the heat sink geometry and the temperatures (T_{hs} & T_{amb}), the achievable $R_{th,hs}$ for natural convection cooling can be calculated. This results in a tradeoff curve between the volume of the heat sink V_{hs} and achievable R_{th} at given temperatures (T_{amb}&T_{hs}) as shown in Fig. 6(b). The minimal volume for a natural convection and the desired $R_{th,hs}$ can directly be evaluated from this curve.

Combining both kinds of cooling results in a Pareto curve for a predefined T_j and $R_{th,hs}$ with the volume of the heat sink V_{hs} and the power consumption of the fan P_{fan} (down to zero) as key parameters as shown in Fig. 9. The gray dotted surface illustrates the achievable $R_{th,hs}$ for different fan powers P_{fan} and volumes V_{hs}. The gray plane represents the desired $R_{th,hs}$ which is in this example at 0.4 K/W. The optimal combination between P_{fan} and V_{hs} for achieving a defined $R_{th,hs}$ results from the intersection between these surfaces (black line in Fig. 9). The minimum achievable volume is defined by the considered design space, which is higher for forced convection heat sinks than for natural convection heat sinks due to the additional volumes of the fan and the adapter. Obviously the required heat sink volume becomes smaller with increasing fan power. However, especially at high fan powers, only a slightly lower V_{hs} can be achieved.

If the required $R_{th,hs}$ is increased, the gray plane is shifted upward. At the intersection point between the mechanical limit and the free convection limit, natural convection would be sufficient to achieve a thermal feasible design. For higher $R_{th,hs}$, even lower volumes than with forced convection cooling can be achieved (indicated red in Fig. 9).

This means by increasing the required $R_{th,hs}$ (e.g., lowering the losses by paralleling semiconductor devices), not only the minimum required fan power decreases and thus the overall system efficiency increases, but also a reduced V_{hs} could be achieved by enabling natural convection. The question would be how much volume is lost by the additional devices compared to the additional volume introduced by the fan and the adapter.

Fig. 10(a) depicts the maximum allowed thermal resistance $R_{th,hs,\max}$ for the heat sink as function of the number of paralleled semiconductor devices for the half-bridge converter in buck operation for the considered operating point (see Fig. 1 & Table II). As can be seen in Fig. 10(b), by only paralleling two devices, a natural convection heat sink would already be sufficient since the conduction losses of a single device are reduced by a factor of ≈ 4. Referring to Fig. 9, this is approximately the intersection point of the mechanical limit and the free convection and actually states the boundary where natural convection becomes beneficial in terms of volume compared to forced convection.

If three devices are paralleled, not only the system efficiency can be improved but also the volume of the natural convection heat sink becomes smaller than the minimal volume achieved by forced convection. Paralleling more than five devices would result in a higher volume because of the increased mounting area required for the semiconductors A_{semi} [indicated in Fig. 10(b) as A_{semi} driven]. Additionally, increasing losses P_{tot} can be observed by paralleling more than seven devices due to increasing switching losses [sum of all switching losses Fig. 10(a)].

B. *Variable Junction Temperature* $T_j < T_{j,\max}$

Since colder devices are more efficient, a smaller $R_{th,hs}$ enables lower semiconductor losses and instead of optimizing a heat sink for a fixed T_j, it may be beneficial to only limit the

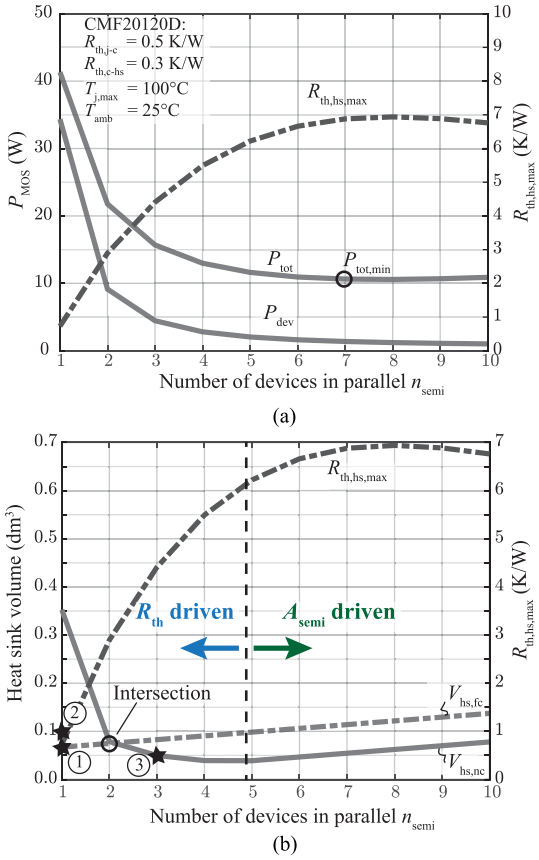

Fig. 10. (a) P_{semi} and $P_{\mathrm{dev,max}}$ for the considered operating point in dependence of paralleled semiconductors n_{semi}. The required $R_{th,hs}$ is increasing with decreasing losses. (b) Minimum heat sink volume for natural convection cooling to achieve a thermal feasible heat sink design. For three devices a reduced volume compared to forced convection cooling can be observed. For more than five devices the volume is not anymore defined by the $R_{th,hs}$ (R_{th}-driven) but by the number of semiconductors that have to be mounted on the baseplate of the heat sink (A_{semi}-driven).

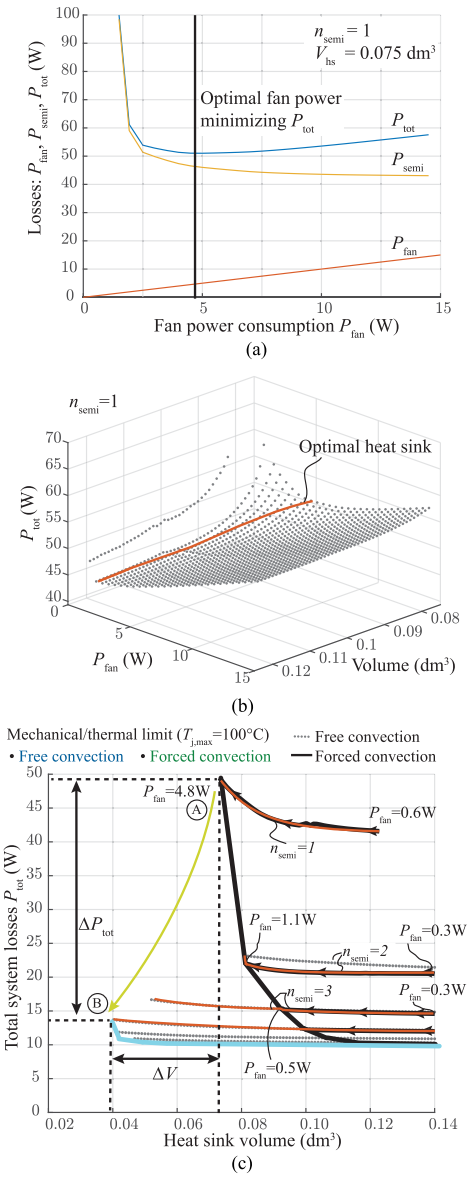

Fig. 11. (a) Losses of the semiconductor devices P_{semi} in dependence of the applied fan power P_{fan} at a given volume. The optimal applied fan power minimizing P_{tot} is approximately around 5W. (b) Overall losses can be calculated for every volume V_{hs} and P_{fan} for a defined number of paralleled devices n_{semi}, what results in optimal combination of P_{fan} and V_{hs} minimizing P_{tot} (indicated red). (c) Combination of this tradeoff curves for different n_{semi} for forced and natural convection heat sinks (red indicated) if the junction temperature is not fixed ($T_{\mathrm{amb}} < T_j < T_{j,\mathrm{max}}$). The power values ($P_{\mathrm{fan}} = 4.8 \ldots 0.3$ W) represent the optimal fan power for the respective heat sink design/volume employing forced convection cooling. The black and the blue line represent the limits of the heat sink designs due to thermal boundaries ($T_j < 100$ °C) or mechanical boundaries (see Table III). The heat sink volume as well as the overall efficiency can be improved by natural convection cooling heat sinks as indicated with the yellow line (design for forced Ⓐ and natural Ⓑ convection).

maximum $R_{th,hs,\mathrm{max}}$. To investigate what could be gained in terms of conduction losses by providing a higher P_{fan}, enabling a lower $R_{th,hs}$, the optimization routine has to be modified by an internal iteration loop for forced as well as for natural convection cooling (see Fig. 8). For the forced convection cooling, for every heat sink geometry, the achievable $R_{th,hs}$ is calculated in dependence of the applied P_{fan} according to the fan laws as discussed in Section II-A. To determine the overall losses P_{tot}, an internal iteration loop (dark grey Fig. 8) has to be integrated, whereas for every $R_{th,hs}$, the temperatures and the according conduction losses have to be recalculated until the temperature deviation is below a certain error limit $\Delta T_{j,\mathrm{err}}$.

For natural convection, $R_{th,hs}$ is also temperature dependent. As a consequence, not only the losses have to be recalculated but also $R_{th,hs}$ has to be adjusted for the actual temperatures $T_{j,op,\mathrm{new}}$.

Taking the overall losses ($P_{\mathrm{tot}} = P_{\mathrm{fan}} + P_{\mathrm{semi}}$) into account, an optimal heat sink design minimizing P_{tot} can be found as indicated in Fig. 11(a) and (b). Obviously, fans with a comparably high power do not always result in an optimal heat sink design since their power consumption is higher than what is gained by the lower junction temperature of the semiconductors.

If the overall efficiency is taken into account and only the upper boundary of the junction temperature $T_{j,\mathrm{max}}$ is fixed, the efficiency can be improved by applying fans due to the reduced $R_{ds,\mathrm{on}}$ of colder devices. In Fig. 11(c), this effect is taken into account to determine the optimal cooling system for different number of devices, whereas $T_{\mathrm{amb}} < T_j < T_{j,\mathrm{max}} =$

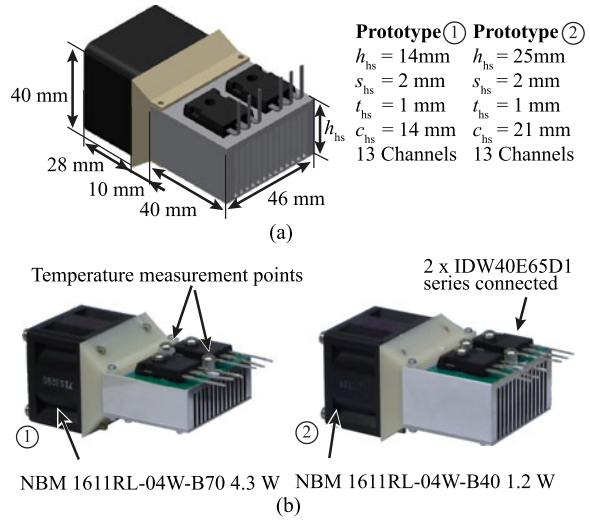

Fig. 12. (a) Geometrical parameters of the two forced convection prototype systems to validate the theoretical calculations. (b) Two prototype heat sinks and the used elements for the tests. The numbers ① and ② are used to identify the prototype systems in the theoretical considerations.

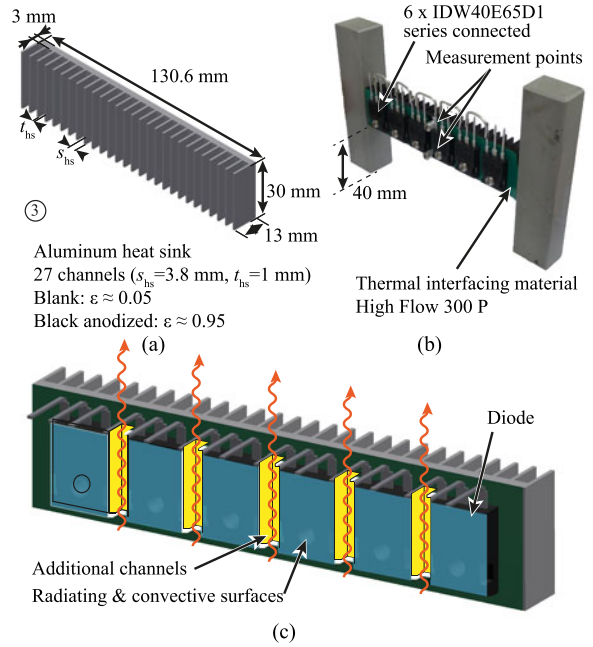

Fig. 13. (a) Geometrical dimensions of the prototype system for natural convection ②. There, one heat sink is black anodized and the other blank. (b) Measurement setup for the validation of the analytical models. (c) Additional considered convecting and radiating surfaces are indicated.

100 °C. By paralleling three devices, the efficiency gain because of the reduced device temperature is approximately equal or less than the fan power consumption and the two loss curves for forced and natural convection are approximately the same [see Fig. 11(c)]. Since for natural convection heat sinks, no volume for the fan and the cross section adapter is required, the volume can be further reduced. This results in an efficiency and power density gain for natural convection compared to forced convection as indicted by Ⓐ → Ⓑ in Fig. 11. However, this gain is always linked to an increasing amount of semiconductor devices and thus to higher costs and complexity.

IV. Validation of the Models

To validate the analytical heat sink models and the results, four prototype heat sinks have been built. The dimensions are given in Figs. 12 and 13. To generate the heat flux in the heat sinks, two respectively six series connected diodes (IDW40E65D1) have been mounted and supplied with a constant forward current. Since these diodes have a negative temperature coefficient in the considered current range, the temperature of the devices/on the heat sink is self-stabilizing. The temperatures of the ambient and of the heat sink base plate were measured with type-K thermocouples. The results for the forced convection cooling can be found in Table IV. The thermal resistance fits quite well to the analytical results. However, the power consumption of the fans is increased compared to the optimal determined power consumption due to the significant variance of the fan efficiency (see Fig. 4). Due to the comparably high thermal resistance of the free convection heat sink, additional convecting and radiating surfaces have to be considered for the measurement [see Fig. 13(c)]. In the measurement setup, the semiconductors constitute also a finned structure and the devices are radiating ($R_{th,ad}$). The three columns on the right-hand side show the theoretically calculated thermal resistances of the heat sink $R_{th,hs}$ and the setup $R_{th,ad}$ and the resulting total thermal resistance $R_{th,\mathrm{tot}}$. Thermal tests include blank and anodized heat sink in which the fins are vertically [see Fig. 13(b)] and horizontal upward arranged, where the heat sink and the ambient temperature as well as the power losses of the diodes were measured. The measurements were executed for about 30 min per measurement point to reach the thermal equilibrium. The measurement results are summarized in Table V. For all test setups, a reduction of the $R_{th,\mathrm{tot}}$ with increasing temperature difference can be observed. Furthermore, by anodizing the heat sink black, the $R_{th,\mathrm{tot}}$ can be reduced by approximately 15%. The arrangement of the heat sink (vertically or horizontally) has an impact of another 10% on the thermal resistance. The best results concerning the $R_{th,\mathrm{tot}}$ were achieved by black anodized vertically arranged heat sinks. The measurements match well to the theoretical calculations.

TABLE IV
Measurement Results for Forced Convection Cooling

		Prototype ①	Prototype ②
Heat sink volume	V	0.076 dm^3	0.089 dm^3
Power of the fan	P_{fan}	3.3 W	1.13 W
Calc. thermal resistance	$R_{th,\mathrm{calc}}$	0.6 K/W	0.6 K/W
Calc. power consumption	$P_{\mathrm{fan,calc}}$	3.1 W	0.75 W
Total diode power losses	P_{semi}	43.9 W	43.8 W
Ambient temperature	T_{amb}	24.6 °C	24.0 °C
Heat sink temperature	T_{hs}	50.5 °C	50.8 °C
Measured thermal resistance	$R_{th,\mathrm{meas}}$	0.59 K/W	0.61 K/W

TABLE V
MEASUREMENT RESULTS FOR NATURAL CONVECTION COOLING FOR CASE STUDY ③

Measurements				Calculations		
T_{amb} °C	T_{hs} °C	P_{semi} W	$R_{th,m}$ K/W	$R_{th,\mathrm{tot}}$ K/W	$R_{th,hs}$ K/W	$R_{th,ad}$ K/W
black anodized, vertically arranged						
23.9	60.2	8.99	**4.02**	**4.06**	5.19	18.72
24.8	68.2	11.38	**3.81**	**3.74**	4.73	17.90
25.2	75.4	13.80	**3.63**	**3.51**	4.41	17.30
blank, vertically arranged						
23.5	62.9	8.90	**4.42**	**4.42**	5.84	18.18
24.8	71.3	11.25	**4.16**	**4.05**	5.28	17.38
black anodized, horizontally arranged						
24.8	62.5	8.94	**4.21**	–	–	–
25.0	71.1	11.30	**4.07**	–	–	–

V. CONCLUSION

In highly efficient converter systems, the power consumption of the cooling system could have a significant impact on the overall system efficiency. Especially for highly efficient systems, it is important to include the power consumption of the fans in the efficiency analysis since high power fans do not necessarily result in the highest system efficiency. Therefore, in this paper, the theoretical models for forced convection cooling are extended by the power of the fan. Furthermore, a modeling and optimization concept for free convection cooling is presented and validated with prototype systems. A good matching between the measurements and the calculations with a deviation of less than 5% was observed for the considered prototypes.

With the models, the theoretical limits of forced and free convection cooling are discussed based on the example of a half-bridge converter. There, also the temperature dependent on-state resistance of the devices is taken into account. In specific cases, the efficiency as well as the power density of the overall system can be improved by employing natural convection heat sinks instead of forced convection. In the considered case, the losses can be reduced by factor of 3 and the corresponding heat sink volume can be reduced by 50% by paralleling semiconductor devices.

However, to enable a thermally feasible design employing natural convection, a high amount of semiconductor devices is required. This reduces the problem to how much volume is lost by additional semiconductor devices compared to the volume required for the fans. Furthermore, its performance strongly depends on the occurring temperatures (ambient, heat sink temperature) and on the installation position.

Thus, natural convection heat sinks are an attractive solution for fixed installations (e.g., solar farms, EV charging stations), where the heat sinks can be arranged such that the air flow is not influenced by other heat sources and a high efficiency is required. For installations in a cabinet (e.g., server stations), where no thermal decoupling can be assumed, a shared fan at the inlet or outlet of the cabinet could be sufficient, since already a small air flow significantly reduces the thermal resistance.

REFERENCES

[1] S. Y. Kim and R. L. Webb, "Analysis of convective thermal resistance in ducted fan-heat sinks," *IEEE Trans. Compon. Packag. Technol.*, vol. 29, no. 3, pp. 439–448, 2006.

[2] W. M. Rohsenow *et al.*, *Handbook of Heat Transfer*, vol. 3. New York, NY, USA: McGraw-Hill, 1998.

[3] A. Bejan and A. D. Kraus, *Heat Transfer Handbook*, vol. 1. New York, NY, USA: Wiley, 2003.

[4] H. D. Baehr and K. Stephan, *Wärme-und Stoffübertragung*, vol. 6. New York, NY, USA: Springer, 1994.

[5] U. Drofenik and J. W. Kolar, "Analyzing the theoretical limits of forced air-cooling by employing advanced composite materials with thermal conductivities," in *Proc. 4th Int. Conf. Integrated Power Syst.*, Jun. 2006, pp. 1–6.

[6] U. Drofenik, A. Stupar, and J. W. Kolar, "Analysis of theoretical limits of forced-air cooling using advanced composite materials with high thermal conductivities," *IEEE Trans. Compon., Packag. Manuf. Technol.*, vol. 1, no. 4, pp. 528–535, Apr. 2011.

[7] C. Gammeter, F. Krismer, and J. W. Kolar, "Weight optimization of a cooling system composed of fan and extruded-fin heat sink," *IEEE Trans. Ind. Appl.*, vol. 51, no. 1, pp. 509–520, Jan./Feb. 2015.

[8] Y. Muzychka and M. Yovanovich, "Laminar forced convection heat transfer in the combined entry region of non-circular ducts," *J. Heat Transfer*, vol. 126, no. 1, pp. 54–61, 2004.

[9] Y. Muzychka and M. Yovanovich, "Pressure drop in laminar developing flow in noncircular ducts: A scaling and modeling approach," *J. Fluids Eng.*, vol. 131, no. 11, 2009, Art. no. 111105.

[10] Y. S. Muzychka, "Generalized models for laminar developing flows in heat sinks and heat exchangers," *Heat Transfer Eng.*, vol. 34, nos. 2-3, pp. 178–191, 2013.

[11] F. M. White *et al.*, *Fluid Mechanics*, vol. 7. New York, NY, USA: McGraw-Hill, 2003.

[12] D. Copeland, "Optimization of parallel plate heatsinks for forced convection," in *Proc. 16th Annu. IEEE Semicond. Thermal Meas. Manage. Symp.*, 2000, pp. 266–272.

[13] D. W. Copeland, "Fundamental performance limits of heatsinks," *J. Electron. Packag.*, vol. 125, no. 2, pp. 221–225, 2003.

[14] P. Canhoto and A. H. Reis, "Optimization of forced convection heat sinks with pumping power requirements," *Int. J. Heat Mass Transfer*, vol. 54, no. 7, pp. 1441–1447, 2011.

[15] D. Van De Pol and J. Tierney, "Free convection nusselt number for vertical u-shaped channels," *J. Heat Transfer*, vol. 95, no. 4, pp. 542–543, 1973.

[16] A. Bar-Cohen and W. Rohsenow, "Thermally optimum spacing of vertical, natural convection cooled, parallel plates," *J. Heat Transfer*, vol. 106, no. 1, pp. 116–123, 1984.

[17] A. Bar-Cohen, M. Iyengar, and A. D. Kraus, "Design of optimum plate-fin natural convective heat sinks," *J. Electron. Packag.*, vol. 125, no. 2, pp. 208–216, 2003.

[18] K. H. Do, T. H. Kim, Y.-S. Han, B.-I. Choi, and M.-B. Kim, "General correlation of a natural convective heat sink with plate-fins for high concentrating photovoltaic module cooling," *Sol. Energy*, vol. 86, no. 9, pp. 2725–2734, 2012.

[19] J. R. Welling and C. Wooldridge, "Free convection heat transfer coefficients from rectangular vertical fins," *J. Heat Transfer*, vol. 87, no. 4, pp. 439–444, 1965.

[20] J. R. Culham, M. M. Yovanovich, and S. Lee, "Thermal modeling of isothermal cuboids and rectangular heat sinks cooled by natural convection," *IEEE Trans. Compon., Packag. Manuf. Technol. A*, vol. 18, no. 3, pp. 559–566, Sep. 1995.

[21] P. Teertstra, M. Yovanovich, and J. Culham, "Analytical forced convection modeling of plate fin heat sinks," *J. Electron. Manuf.*, vol. 10, no. 4, pp. 253–261, 2000.

[22] G. Mirzaeva and L. Sazdanoff, "The effect of flux optimization on energy efficiency of induction motors in fan and pump applications," in *Proc. 2015 Aust. Univ. Power Eng. Conf.*, 2015, pp. 1–6.

[23] V. Martin and M. Falk, "Optimizing the performance and reliability of process fans: Achieve success and avoid problems by implementing the right strategy," in *Proc. IEEE Cement Ind. Tech. Conf.*, 2006, 14 pp.

[24] Elementary Fan Technology, 2016. [Online]. Available: www.tlt-turbo.com

[25] S. Yen and F. K. Lin, "Exit flow field and performance of axial flow fans," *J. Fluids Eng.*, vol. 128, no. 2, pp. 332–340, 2006.

[26] N. Smith, "High efficiency electronic cooling fans," in *Proc. IEEE Semicond. Thermal Meas. Manage. Symp.*, 2009, pp. 92–97.

[27] H. Osawa, "Fan basics and selection criteria (how to use)," SANYO DENKI Corporation, Ltd., Tech. Rep. 40, 2015.
[28] D. Leuenberger and J. Biela, "Comparison of a soft switched tcm t-type inverter to hard switched inverters for a 3 phase PV grid interface," in *Proc. 15th Int. IEEE Power Electron. Motion Control Conf.*, 2012, pp. LS1d.1-1–LS1d.1-8.
[29] "Fischer Elektronik GmbH & Co. KG," 2016. [Online]. Available: http://www.fischerelektronik.de/

Daniel Christen (S'12) received the M.Sc. degree in electrical engineering from the Swiss Federal Institute of Technology Zurich (ETH Zurich), Zurich, Switzerland, in 2009, where he dealt with power electronics and control engineering. He is currently working toward the Ph.D. degree in the Laboratory for High Power Electronic Systems, ETH Zurich, Zurich. His research interest focuses on the modeling and the design of power electronic systems for ultrafast charging stations for EVs with respect to the achievable power density and efficiency.

Milos Stojadinovic (S'14) studied electrical engineering at the School of Electrical Engineering, University of Belgrade, Belgrade, Serbia, focusing on electrical drives and converters. He received the Master's degree in electrical drives and converters, in 2011, where his thesis dealt with means of compensating nonidealities in three-phase inverters. In January 2013, he joined the High Power Electronics Laboratory, where he is working toward the Ph.D. degree, focusing on traction-drive applications.

Juergen Biela (S'04–M'06–SM'16) received the Diploma (Hons.) degree from Friedrich-Alexander Universität Erlangen-Nürnberg, Nuremberg, Germany, in 1999, and the Ph.D. degree from the Swiss Federal Institute of Technology (ETH Zurich), Zurich, Switzerland, in 2006.

He joined the Research Department, Siemens A&D, Erlangen, Germany, in 2000, where he has been involved in inverters with very high switching frequencies, SiC components, and EMC. In 2002, he joined the Power Electronic Systems Laboratory, ETH Zurich, as a Ph.D. student focusing on optimised electromagnetically integrated resonant converters. From 2006 to 2007, he was a Postdoctoral Fellow with the Power Electronic Systems Laboratory, and a Guest Researcher with the Tokyo Institute of Technology, Tokyo, Japan. From 2007 to 2010, he was a Senior Research Associate with the Power Electronic Systems Laboratory. Since 2010, he has been an Associate Professor of high-power electronic systems at ETH Zurich. His current research interests include the design, modeling, and optimisation of PFC, dc–dc, and multilevel converters with an emphasis on passive components, the design of pulsed-power systems, and power electronic systems for future energy distribution.